

Phase estimation via multi-photon subtraction inside the SU(1,1) interferometer

Qingqian Kang^{1,2,*}, Zekun Zhao^{1,*}, Youke Xu¹, Teng Zhao¹, Cunjin Liu¹, and Liyun Hu^{1,3,†}

¹Center for Quantum Science and Technology, Jiangxi Normal University, Nanchang 330022, China

²Department of Physics, Jiangxi Normal University Science and Technology College, Nanchang 330022, China

³Institute for Military-Civilian Integration of Jiangxi Province, Nanchang 330200, China

To improve the phase sensitivity, multi-photon subtraction schemes within the SU(1,1) interferometer are proposed. The input states are the coherent state and the vacuum state, and the detection method is homodyne detection. The effects of multi-photon subtraction on phase sensitivity, quantum Fisher information, and quantum Cramér-Rao bound are analyzed under both ideal and photon losses situations. It is shown that the internal subtraction operation can improve the phase sensitivity, which becomes better performance by increasing subtraction number. It can also efficiently improve the robustness of the SU(1,1) interferometer against internal photon losses. By comparing separately arbitrary photon subtraction on the two-mode inside SU(1,1) interferometer, the performance differences under different conditions are analyzed, including the asymmetric properties of non-Gaussian operations on the phase precision and the quantum Fisher information. Our proposed scheme represents a valuable method for achieving quantum precision measurements.

PACS: 03.67.-a, 05.30.-d, 42.50.Dv, 03.65.Wj

I. INTRODUCTION

Quantum precision measurement, leveraging the unique properties of quantum states, offers a highly accurate approach that has the potential for widespread utilization in diverse fields [1–9], such as quantum computing and quantum communication. Remarkable achievements in quantum measurement technologies have been made, including simultaneous measurement and coherent measurement using quantum entanglement states. These techniques have found applications in biology, physics, and chemistry, enabling improved accuracy in areas such as microbial detection and drug discovery, surpassing classical measurement techniques. Moreover, studying quantum measurement technology not only deepens our understanding of quantum mechanics but also profoundly influences the development of quantum information science. Recognizing that the measurement process itself can introduce disturbances to quantum states, it is essential to identify and mitigate sources of interference, and develop more robust interference cancellation techniques. As the demand for computation and communication continues to grow, the application of quantum measurement technology will expand across various domains. Consequently, the research on quantum precision measurement holds immense value, as it opens up endless opportunities for scientific exploration and technological advancement.

Phase estimation is a critical aspect of precision measurement, with optical interferometers playing a key role in this technique. In 1986, Yurke *et al.* [10] introduced the SU(1,1) interferometer, which replaced traditional beam splitters (BSs) with optical parametric amplifiers

(OPAs). The entangled state generated by the first OPA leads to noiseless amplification during the quantum destructive interference of the SU(1,1) interferometer [11], enhancing the precision of phase estimation. This technique revolutionized phase estimation, becoming a vital tool in quantum precision measurements. By utilizing entangled photon states, the SU(1,1) interferometer can surpass the standard quantum limit (SQL), enabling higher precision. In recent years, there has been significant interest in studying the SU(1,1) interferometer [12]. In 2011, Jing *et al.* [13] successfully implemented this interferometer experimentally. In this nonlinear interferometer, the maximum output intensity can be much higher than that of linear interferometer due to the OPA. Apart from the standard form, various configurations of SU(1,1) interferometer have also been proposed [14–21].

Photon loss inevitably decreases the phase sensitivity during the estimation process, presenting a significant challenge in mitigating its adverse effects. In 2012, Marino *et al.* [22] investigated the impact of losses on the phase sensitivity of the SU(1,1) interferometer with intensity detection. Their findings revealed that although propagation losses reduced phase sensitivity, it was still feasible to surpass the SQL even in the presence of substantial losses. Subsequently, in 2014, Li *et al.* [23] demonstrated that the SU(1,1) interferometer employing coherent and squeezed-vacuum states can approach the Heisenberg Limit (HL) through homodyne detection. Additionally, Manceau *et al.* [24] illustrated that increasing the gain of the second amplifier enables the interferometer to maintain phase supersensitivity despite up to 80% detection losses.

To further fulfill the aforementioned goal, effective methods grounded in non-Gaussian operations, such as photon subtraction [25–27], have been proposed. These operations are notably important in quantum communication and quantum computation [28–31]. They present the potential to generate a more strongly entangled sub-

* These authors contributed equally to this work and should be considered co-first authors.

† Corresponding author. hlyun@jxnu.edu.cn

ensemble from a weakly entangled state [32] and contribute to enhancing quantum measurement precision [33–35]. Experimental studies have illustrated the conditional generation of superpositions of distinct quantum operations through single-photon interference, providing a practical approach for preparing non-Gaussian operations [36]. This advancement has unveiled new possibilities in quantum state manipulation and implications for various quantum technologies.

As previously mentioned, although SU(1,1) interferometer is highly valuable for precision measurement [37, 38], the precision is still affected by dissipation, particularly photon losses inside the interferometer [22, 39]. Consequently, to further enhance precision, non-Gaussian operations should serve as an alternative approach to mitigate internal dissipation. In Reference [40], single-photon subtraction within the SU(1,1) interferometer is utilized to enhance phase sensitivity, thereby increasing robustness against internal losses. Notably, this process only involves the simultaneous subtraction of single photons from two modes.

In this paper, our focus lies in enhancing precision by individually performing arbitrary photon subtraction on the two-mode inside the SU(1,1) interferometer to comprehend the effects of non-Gaussian operations. This includes analyzing the asymmetric properties of non-Gaussian operations on phase precision and the quantum Fisher information (QFI). For instance, it is to understand on which mode multi-photon subtraction scheme works better. The paper is structured as follows. Sec. II outlines the theoretical model of the multi-PSS. Sec. III delves into phase sensitivity, encompassing both the ideal case and the internal photon losses case. Sec. IV centers on the QFI and quantum Cramér-Rao bound (QCRB) [41, 42]. Finally, Sec. V provides a comprehensive summary.

II. MODEL

In this section, we commence by introducing the SU(1,1) interferometer, depicted in Fig. 1(a). Typically, the SU(1,1) interferometer comprises two optical parametric amplifiers (OPAs) and a linear phase shifter, representing one of the most commonly employed interferometers in quantum metrology research. The first OPA is characterized by a two-mode squeezing operator $U_{S_1}(\xi) = \exp(\xi_1^* ab - \xi_1 a^\dagger b^\dagger)$, where a (b), a^\dagger (b^\dagger) represent the photon annihilation and photon creation operators, respectively. The squeezing parameter $\xi_1 = g_1 e^{i\theta_1}$ can be expressed in terms of a gain factor g_1 and a phase shift θ_1 , and plays a critical role in shaping the interference pattern and determining the phase sensitivity of the system. Following the first OPA, mode a undergoes a phase shift process $U_\phi = \exp[i\phi(a^\dagger a)]$, while mode b remains unchanged. Subsequently, the two beams are coupled in the second OPA with the operator $U_{S_2}(\xi) = \exp(\xi_2^* ab - \xi_2 a^\dagger b^\dagger)$, where $\xi_2 = g_2 e^{i\theta_2}$ and $\theta_2 - \theta_1 = \pi$.

In the proposed scheme, $g_1 = g_2 = g$, and we utilize coherent state $|\alpha\rangle_a$ and vacuum state $|0\rangle_b$ as input states. Homodyne detection on the a -mode of the output is employed.

The SU(1,1) interferometer is generally susceptible to photon losses, particularly in the case of internal losses. To simulate photon losses, the use of fictitious BS is proposed, as depicted in Fig. 1(a). The operators of these fictitious BSs can be described as $U_B = U_{B_a} \otimes U_{B_b}$, with $U_{B_a} = \exp[\theta_a (a^\dagger a_v - a a_v^\dagger)]$ and $U_{B_b} = \exp[\theta_b (b^\dagger b_v - b b_v^\dagger)]$, where a_v and b_v represent vacuum modes. Here, T_k (where $(k = a, b)$) denotes the transmissivity of the fictitious BSs, associated with θ_k through $T_k = \cos^2 \theta_k \in [0, 1]$. A transmissivity value of ($T_k = 1$) corresponds to the ideal case without photon losses [43]. In an expanded space, the expression for the output state of the standard SU(1,1) interferometer can be represented as the following pure state, i.e.,

$$|\Psi_{out}^0\rangle = U_{S_2} U_\phi U_B U_{S_1} |\alpha\rangle_a |0\rangle_b |0\rangle_{a_v} |0\rangle_{b_v}. \quad (1)$$

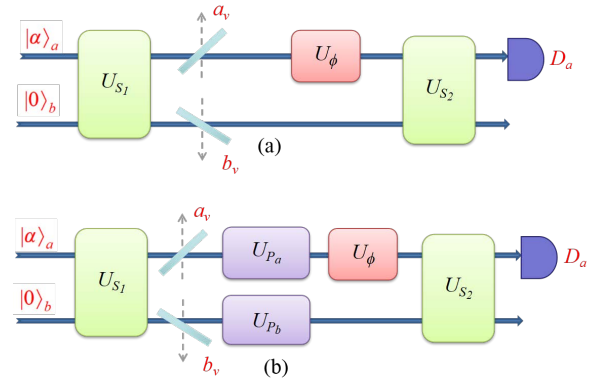


FIG. 1. Schematic diagram of the SU(1,1) interferometer. (a) the standard SU(1,1) interferometer, (b) the SU(1,1) interferometer with multi-PSS. The two input ports are a coherent state $|\alpha\rangle_a$ and a vacuum state $|0\rangle_b$. a_v and b_v are vacuum modes. U_{S_1} and U_{S_2} are the optical parametric amplifier, U_ϕ is the phase shifter. U_P is the multi-photon subtraction operation and D_a is the homodyne detector.

To mitigate the impact of photon losses, following the first OPA, we introduce the multi-PSS on the two modes within the SU(1,1) interferometer, illustrated in Fig. 1(b). In the multi-PSS, m and n photons are subtracted from mode a and mode b , respectively. This process can be described by the operator $U_P = a^m \otimes b^n$. Consequently, the output state of the interferometer can be expressed in the following form

$$|\Psi_{out}^1\rangle = A U_{S_2} U_\phi U_P U_B U_{S_1} |\alpha\rangle_a |0\rangle_b |0\rangle_{a_v} |0\rangle_{b_v}. \quad (2)$$

The normalization constant for the multi-PSS, denoted by A , is given by [43]

$$A^{-2} = D_{m_1, n_1, m_2, n_2} e^{w_1}, \quad (3)$$

where $D_{m_1, n_1, m_2, n_2} = \partial^{m_1+n_1+m_2+n_2} / \partial \lambda_1^{m_1} \partial \lambda_2^{n_1} \partial \lambda_3^{m_2} \partial \lambda_4^{n_2} (\cdot) |_{\lambda_1=\lambda_2=\lambda_3=\lambda_4=0}$, and

$$w_1 = u_1 u_2 + u_3 u_4 + u_3 \alpha \quad (4)$$

$$+ \left(\lambda_1 \sqrt{T_k} \cosh g + u_4 \right) \alpha^*, \quad (5)$$

$$u_1 = -\lambda_1 \sqrt{T_k} e^{-i\theta_1} \sinh g, \quad (6)$$

$$u_2 = \sqrt{T_k} (\lambda_2 \cosh g - \lambda_3 e^{i\theta_1} \sinh g), \quad (7)$$

$$u_3 = \sqrt{T_k} (\lambda_3 \cosh g - \lambda_2 e^{-i\theta_1} \sinh g), \quad (8)$$

$$u_4 = -\lambda_4 \sqrt{T_k} e^{i\theta_1} \sinh g. \quad (9)$$

III. PHASE SENSITIVITY

Quantum metrology, an effective approach utilizing quantum resources for precise phase measurements [44, 45], aims to achieve highly sensitive measurements of unknown phases. In this section, we further investigate the phase sensitivity for the multi-PSS within the SU(1,1) interferometer [46]. Various detection methods are available for this purpose, such as homodyne detection [47, 48], parity detection [49, 50], and intensity detection [51]. Each of these methods offers different trade-offs between sensitivity, complexity, and practical implementation. It is important to note that for different input states and interferometers, the phase sensitivities of various detection schemes may be different [52].

Here, we take homodyne detection as the detection method of the output a due to the fact that it is often the most straightforward method to implement experimentally. In homodyne detection, the measured variable is one of the two orthogonal components of the mode a , i.e., $X = (a + a^\dagger) / \sqrt{2}$. According to the error propagation equation [10], the phase sensitivity can be written as

$$\Delta\phi = \frac{\sqrt{\langle \Delta^2 X \rangle}}{|\partial \langle X \rangle / \partial \phi|} = \frac{\sqrt{\langle X^2 \rangle - \langle X \rangle^2}}{|\partial \langle X \rangle / \partial \phi|}. \quad (10)$$

Based on Eqs. (2) and (10), the phase sensitivity for the multi-PSS can be theoretically determined. The detail calculation steps for the phase sensitivity $\Delta\phi$ of the multi-PSS are provided in Appendix A.

A. Ideal case

First, we explore the ideal case, corresponding to $T_k = 1$ (where $(k = a, b)$), i.e., without photon losses. For different numbers of photons subtracted, we depict the phase sensitivity $\Delta\phi$ as a function of ϕ in Fig. 2, including single-mode photon subtraction (Fig. 2(b)), as well as symmetrical and asymmetrical two-mode photon subtraction (Fig. 2(a) and (c)). The observations derived from Fig. 2 are as follows. (i) The phase sensitivity initially improves and then diminishes as the phase increases, with the optimal sensitivity deviating from

$\phi = 0$. (ii) It is noteworthy that photon subtraction within the SU(1,1) interferometer effectively enhances the phase sensitivity $\Delta\phi$, particularly with an increased number of subtracted photons on both modes. (iii) In the case of single-mode photon subtraction, it is evident that the performance of photon subtraction from mode b surpasses that from mode a at small phase values, while the reverse holds true at larger phase values (see Fig. 2(b)). (iv) Similarly, this observation applies to asymmetrical two-mode photon subtraction (refer to Fig. 2(c)), indicating the asymmetric impact of photon subtraction on modes a and b , with the optimal sensitivity achieved through photon subtraction from mode a .

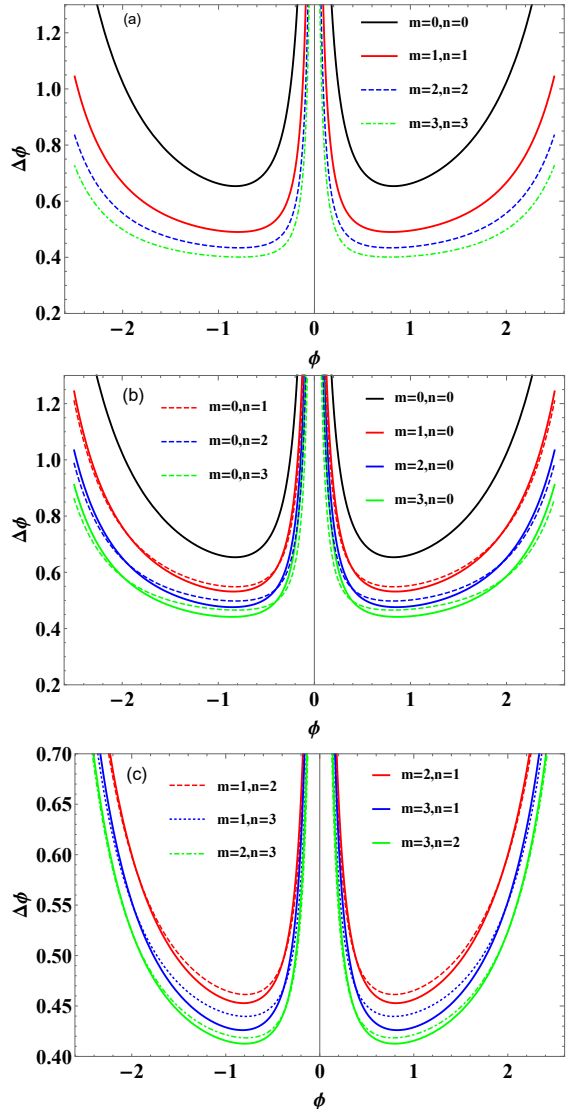


FIG. 2. The phase sensitivity of multi-PSS based on the homodyne detection as a function of ϕ with $\alpha = 1$ and $g = 1$. (a) symmetrical two-mode multi-PSS, (b) single mode multi-PSS, (c) Arbitrary multi-PSS.

In Fig. 3, the phase sensitivity $\Delta\phi$ is plotted as a function of the gain factor g for different numbers of sub-

tracted photons. The plot demonstrates that the phase sensitivity is enhanced with an increase in the gain factor g , and this improvement is further enhanced with an increase in the number of subtracted photons. Particularly noteworthy from Fig. 3(b) is the observation that the multi-PSS on mode b exhibits higher phase sensitivity than that on mode a when the value of g is small, while the reverse is true when the value of g is large. Furthermore, in the case of asymmetrical multi-PSS on mode b , the change in phase sensitivity is relatively flat with increasing g . Conversely, for the asymmetrical multi-PSS on mode a , the enhancement in phase sensitivity initially improves and then diminishes with the gain factor g .

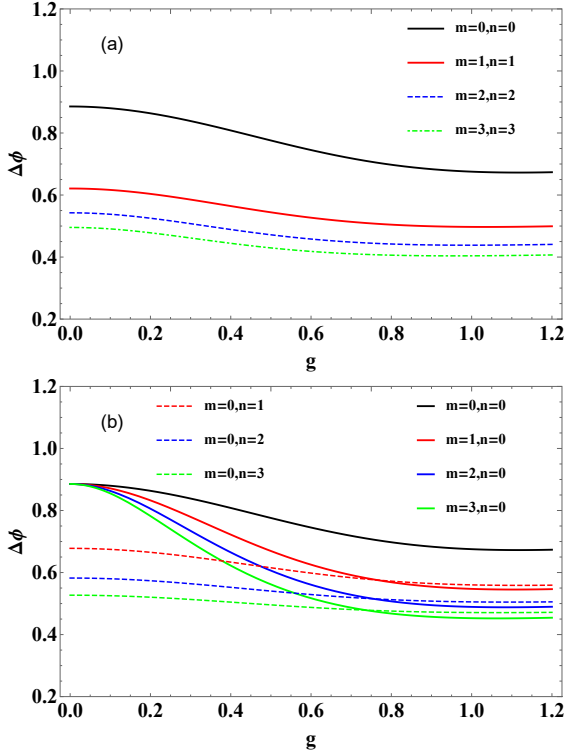


FIG. 3. The phase sensitivity as a function of g , with $\alpha = 1$ and $\phi = 0.6$. (a) symmetrical two-mode multi-PSS, (b) single mode multi-PSS.

Similarly, we examine the phase sensitivity $\Delta\phi$ as a function of the coherent amplitude α , as illustrated in Fig. 4. Several similar findings are observed compared to those in Fig. 3. For example, the phase sensitivity exhibits improvement with the coherent amplitude α , which can be attributed to an increase in the average photon number with α . Moreover, the enhancement effect initially grows and then diminishes with the coherent amplitude α and the number of subtracted photons. Once again, the asymmetrical property of multi-PSS on modes a and b is evident. Notably, as depicted in Fig. 4(b), the multi-PSS on mode a yields higher phase sensitivity than that on mode b in a smaller region of α , whereas the converse holds true in a larger region of α . These findings indicate that the selection of the mode for

implementing the multi-PSS depends on the specific parameters and requirements of the measurement task.

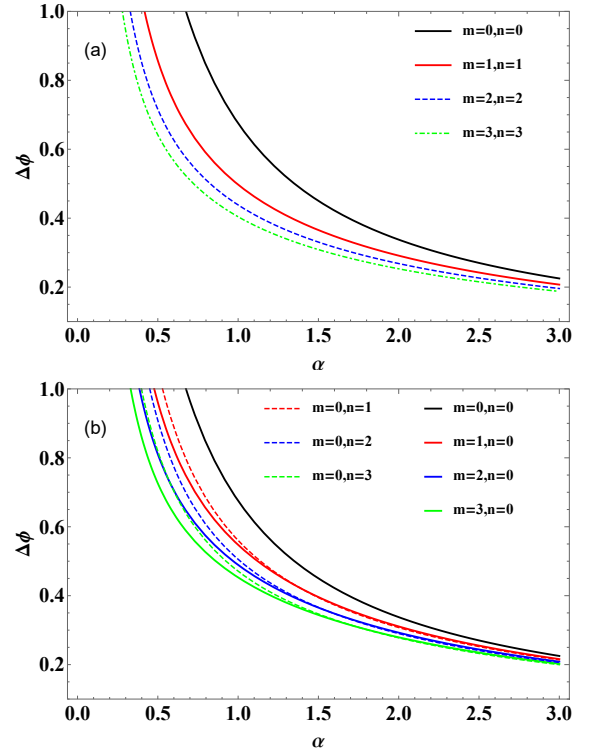


FIG. 4. The phase sensitivity as a function of α , with $g = 1$ and $\phi = 0.6$. (a) symmetrical two-mode multi-PSS, (b) single mode multi-PSS.

B. Photon losses case

The SU(1,1) interferometer plays a critical role in achieving high-precision measurements. However, precision is significantly affected by photon losses, especially internal losses. Now, we pay our attention to the internal photon losses, corresponding to $T_k \in (0, 1)$. The phase sensitivity is plotted as a function of transmittance T_k in Fig. 5 for fixed g , α , ϕ , with varying numbers of subtracted photons. As anticipated, the phase sensitivity is enhanced with increasing transmittance T_k because lower transmittance corresponds to higher levels of internal losses, which weaken the performance of phase estimation. The improved effects of phase sensitivity are also evident with an increase in the number of subtracted photons. Furthermore, it is noteworthy that the multi-PSS on mode b yields higher phase sensitivity than that on mode a in a highly dissipative region (approximately $> 70\%$), while the reverse is true in a low dissipative region (approximately $< 30\%$). However, the sensitivity difference is not significant for the latter case. This suggests that the single-mode multi-PSS on mode b exhibits more robustness than that on mode a against large

internal photon losses.

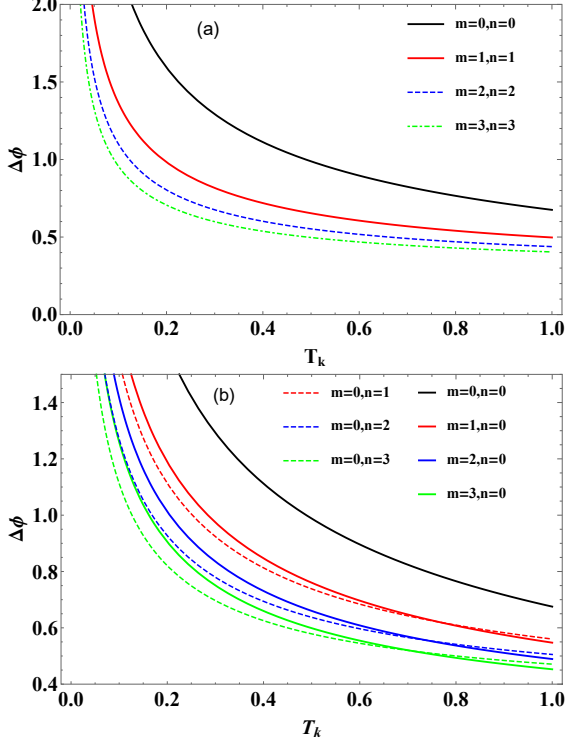


FIG. 5. The phase sensitivity as a function of transmittance T_k , with $g = 1$, $\phi = 0.6$ and $\alpha = 1$. (a) symmetrical two-mode multi-PSS, (b) single mode multi-PSS.

C. Comparison with SQL

Additionally, we compare the phase sensitivity with the SQL and the HL in this subsection. The SQL and HL are defined as $\Delta\phi_{SQL} = 1/\sqrt{N}$ and $\Delta\phi_{HL} = 1/N$, respectively, where N represents the total mean photon number inside the interferometer before the second OPA for each scheme [53–55]. N can be calculated as

$$\begin{aligned} N &= A^2 \langle \Psi_{in} | U_{S_1}^\dagger U_B^\dagger U_P^\dagger (a^\dagger a + b^\dagger b) \\ &\quad \times U_P U_B U_{S_1} | \Psi_{in} \rangle \\ &= A^2 [D_{m_1+1, n_1, m_2+1, n_2} e^{w_1} \\ &\quad + D_{m_1, n_1+1, m_2, n_2+1} e^{w_1}]. \end{aligned} \quad (11)$$

In our schemes, we set the total mean photon number $N = 4$ for all interferometers and compared the phase sensitivity $\Delta\phi$ with the SQL and the HL, as depicted in Fig. 6. Our findings demonstrate that (i) the original state (without multi-PSS) cannot surpass the SQL. (ii) Within a wide range, the multi-PSS is capable of surpassing the SQL even in the presence of significant photon losses (Fig. 6(b) and (c)). Additionally, the multi-PSS can successfully surpass the SQL even for relatively high internal losses ($T_k = 0.5$). This suggests that the multi-

PSS exhibits better robustness against internal photon losses.

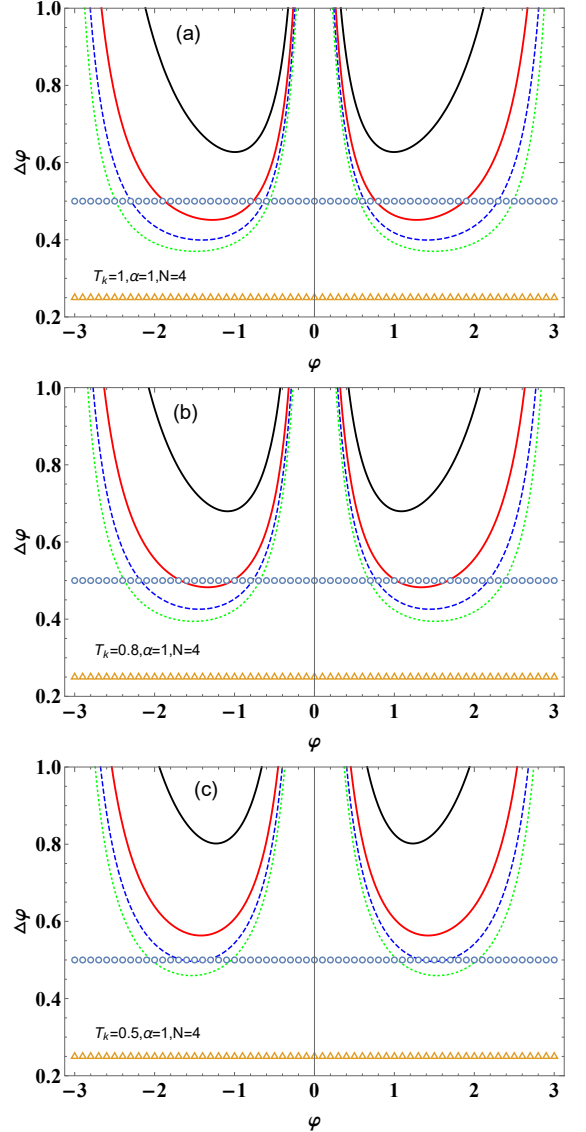


FIG. 6. Comparison of the phase sensitivity with SQL and HL. In the figure, the blue circle is SQL and the yellow triangle is HL. The black solid line corresponds to the standard SU (1,1) interferometer, the red solid line, the blue dashed line and the green dotted line correspond to the simultaneous deduction of one photon, two photons and three photons from the dual modes, respectively.

IV. THE QUANTUM FISHER INFORMATION

In the preceding discussions, we have examined the impact of multi-PSS on phase sensitivity and the correlation between phase sensitivity and relevant parameters based on homodyne detection. It is important to note that the phase sensitivity discussed above is contingent

on the chosen measurement method. Then, for a given interferometer, how to get the maximum phase sensitivity which does not depend on the specific measurement methods? In this section, we turn our attention to the QFI, which represents the maximum information acquired from the interferometer system, regardless of the specific measurement method. We will cases the QFI under ideal and realistic cases, respectively.

A. Ideal case

For a pure state system, the QFI can be derived by [56]

$$F = 4 \left[\langle \Psi'_\phi | \Psi'_\phi \rangle - |\langle \Psi'_\phi | \Psi_\phi \rangle|^2 \right], \quad (12)$$

where $|\Psi_\phi\rangle$ is the quantum state after phase shift and before the second OPA, and $|\Psi'_\phi\rangle = \partial|\Psi_\phi\rangle/\partial\phi$. Then the QFI can be reformed as [56]

$$F = 4 \langle \Delta^2 n_a \rangle, \quad (13)$$

where $\langle \Delta^2 n_a \rangle = \langle \Psi_\phi | (a^\dagger a)^2 | \Psi_\phi \rangle - (\langle \Psi_\phi | a^\dagger a | \Psi_\phi \rangle)^2$.

In the ideal multi-PSS, the quantum state is given by $|\Psi_\phi\rangle = AU_\phi U_p U_{S_1} |\Psi_{in}\rangle$ with $|\Psi_{in}\rangle = |\alpha\rangle_a \otimes |0\rangle_b$, and $U_p = a^m \otimes b^n$. Thus, the QFI is derived as

$$F = 4[A^2 D_{m_1+2, n_1, m_2+2, n_2} e^{w_1} + A^2 D_{m_1+1, n_1, m_2+1, n_2} e^{w_1} - (A^2 D_{m_1+1, n_1, m_2+1, n_2} e^{w_1})^2]. \quad (14)$$

In the above equations, $T_k = 1$. It is possible to explore the connection between the QFI and the related parameters using Eqs. (14).

Fig. 7 and Fig. 8 depict the QFI as a function of g (α) for a specific α (g). It is evident that a higher value of g (α) corresponds to greater QFI. Additionally, it is observed that the QFI is enhanced for the multi-PSS due to the non-Gaussian operation, and this enhancement further increases with the number of manipulated photons. Furthermore, the multi-PSS exhibits slightly better performance on mode b than on mode a (Fig. 7(b) and 8(b)).

Actually, the QFI can be related with the phase sensitivity via [57]

$$\Delta\phi_{QCRB} = \frac{1}{\sqrt{vF}}, \quad (15)$$

Where v is the number of measurements. For simplicity, we set $v = 1$. Another quantum limit, the QCRB [41, 42], is denoted as $\Delta\phi_{QCRB}$, and it establishes the ultimate limit for a set of probabilities resulting from measurements on a quantum system. It is an estimator implemented asymptotically by a maximum likelihood estimator and provides a detection-independent phase sensitivity.

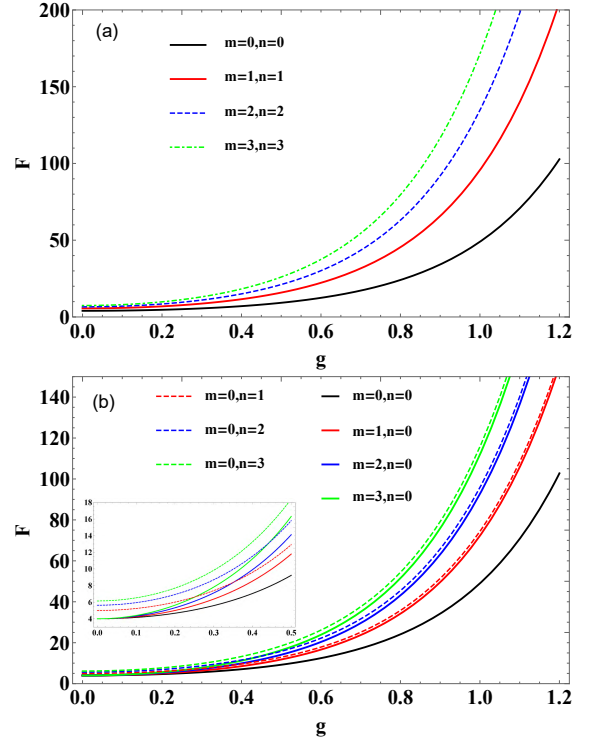


FIG. 7. The QFI as a function of g , with $\alpha = 1$. (a) symmetrical two-mode multi-PSS, (b) single mode multi-PSS.

Fig. 9 and Fig. 10 illustrate the variation of $\Delta\phi_{QCRB}$ as a function of g (α) for a specific α (g). It is shown that $\Delta\phi_{QCRB}$ improves with increasing g and α . Additionally, as the number of photon operations increases, the multi-PSS exhibits greater enhancement for $\Delta\phi_{QCRB}$. Overall, the multi-PSS exhibits better performance on mode b compared to mode a , especially when the gain factor g is smaller (refer to Fig. 9(b)). Furthermore, the improvement in $\Delta\phi_{QCRB}$ is more obvious for small coherent amplitude α (refer to Fig. 10).

In order to acquire a more comprehensive understanding of the impact of the multi-PSS on QFI or $\Delta\phi_{QCRB}$, we have graphed the total mean internal photon number N as a function of the gain factor g and the amplitude α , as illustrated in Fig. 11 and Fig. 12. It is evident that the multi-PSS can increase N as the number of subtracted photons increases. Moreover, the total mean photon number for the multi-PSS on mode b is higher than that on mode a .

B. Photon losses case

In this subsection, we expand our analysis to encompass the QFI in the presence of photon losses. We consider homodyne detection on mode a , which is susceptible to photon losses on mode a . Consequently, our attention is directed toward the QFI of mode a under photon losses, as illustrated in Fig. 13. For realistic quantum

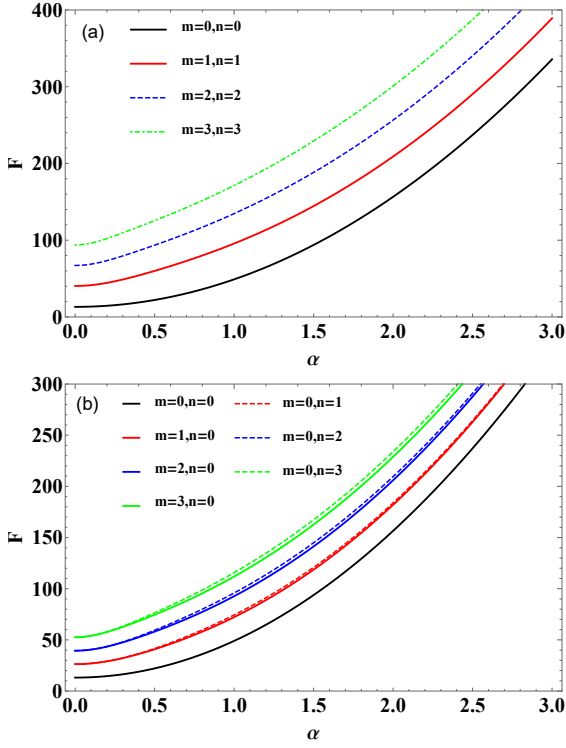


FIG. 8. The QFI as a function of α , with $g = 1$. (a) symmetrical two-mode multi-PSS, (b) single mode multi-PSS.

systems, we have verified the feasibility of computing the QFI with internal non-Gaussian operations by redefining the Kraus operator according to the method proposed by Escher *et al.* [56]. The detailed computational procedure is outlined in Appendix B. Simplifying the calculation process allows us to derive the QFI under photon losses [58].

$$F_L = \frac{4F\eta \langle n_a \rangle}{(1-\eta)F + 4\eta \langle n_a \rangle}, \quad (16)$$

where F is the QFI in the ideal case, and η is the transmittance [59]. Hence, in the presence of photon losses, the QFI in our scheme can be expressed by the following equation

$$F_L = \frac{4F\eta (A^2 D_{m_1+1, n_1, m_2+1, n_2} e^{w_1})}{(1-\eta)F + 4\eta (A^2 D_{m_1+1, n_1, m_2+1, n_2} e^{w_1})}. \quad (17)$$

Under the condition of photon losses, we analyze the effects of each parameter on the QFI to further characterize the degradation of QFI due to photon losses. In Fig. 14, it can be observed that the QFI increases as the transmittance η increases, which is further enhanced as the photon-subtracted number increases. Similar to the ideal case of QFI, this can be attributed to the multi-PSS increasing the number of photons internally, resulting in higher quantum information. It is noteworthy that for both symmetrical and asymmetrical multi-PSS, the im-

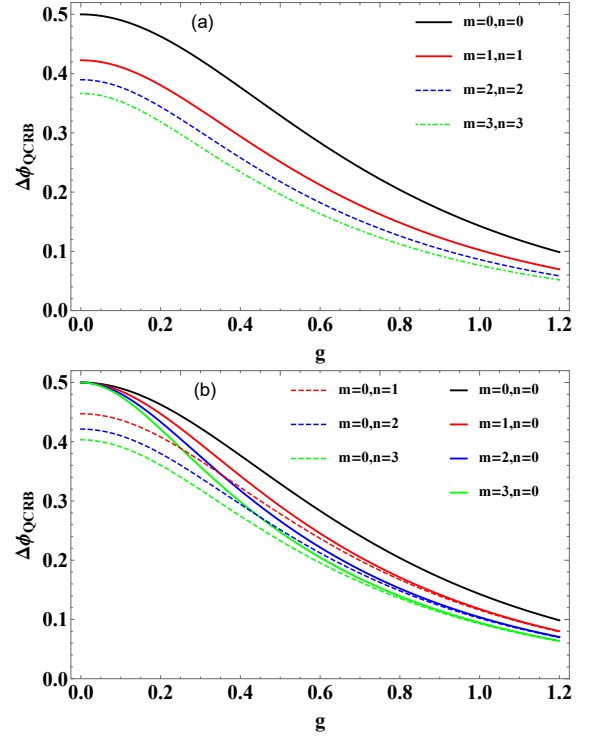


FIG. 9. The $\Delta\phi_{QCRB}$ as a function of g , with $\alpha = 1$. (a) symmetrical two-mode multi-PSS, (b) single mode multi-PSS.

proved QFI increases with the transmittance η . Furthermore, the multi-PSS on mode b exhibits a higher QFI than that on mode a (Fig. 14(b)).

Fig. 15 and Fig. 16 illustrate the QFI as a function of g (α) for a given α (g), with $\eta = 0.8$. In general, the QFI increases as g (α) increases. With an increase in the photon-subtracted number, the multi-PSS exhibits a more pronounced enhancement in QFI. Once more, the QFI of multi-PSS on mode b surpasses that on mode a (refer to Fig. 15(b) and 16(b)). Additionally, for both symmetrical and asymmetrical multi-PSS, the enhanced QFI increases with the gain factor g , while the changes in the enhanced QFI with the coherent amplitude α are insignificant.

Similar to the ideal case, the calculation of $\Delta\phi_{QCRB_L}$ is $\Delta\phi_{QCRB_L} = 1/\sqrt{vF_L}$, with $v = 1$. From Fig. 17, it is evident that the $\Delta\phi_{QCRB_L}$ improves as the transmittance η increases. For the multi-PSS, the $\Delta\phi_{QCRB_L}$ further enhances with the number of subtracted photons. It can be observed that the multi-PSS on mode b exhibits a better $\Delta\phi_{QCRB_L}$ than that on mode a (Fig. 17(b)). Additionally, for both symmetrical and asymmetrical multi-PSS, the improved $\Delta\phi_{QCRB_L}$ initially increases and then decreases with the transmittance η .

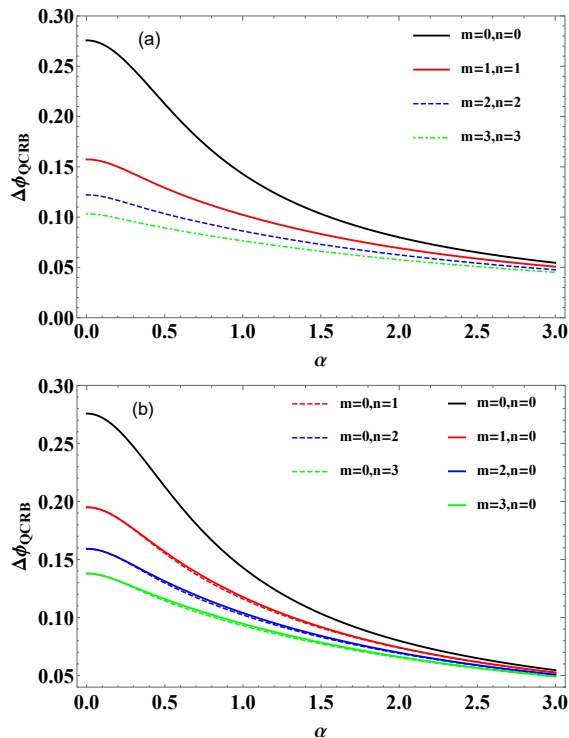


FIG. 10. The $\Delta\phi_{QCRB}$ as a function of α , with $g = 1$. (a) symmetrical two-mode multi-PSS, (b) single mode multi-PSS.

V. CONCLUSION

In this paper, we have not only analyzed the effect of multi-PSS on the phase sensitivity, the QFI and the QCRB in both ideal and real cases, but also compared the results on different modes. Additionally, we have investigated the effects of the gain coefficient g of the parametric amplifier, the coherent state amplitude α and the beam splitter transmittance T_k , which simulates internal photon losses, on the system performance. Through analytical comparison, we have confirmed that the multi-PSS can improve the measurement accuracy of the SU(1,1) interferometer and enhance the robustness to internal photon losses.

The results indicate that increasing the number of operated photons can enhance the phase sensitivity $\Delta\phi$, and more operated photons corresponding to better interferometer performance. The non-Gaussian operation can increase the total mean photon number of the SU(1,1) interferometer, consequently enhancing intramode correlations and quantum entanglement between the two modes. Additionally, we analyze the effects of performing separately arbitrary photon subtraction on the two-mode inside SU(1,1) interferometer, including the asymmetric properties of non-Gaussian operations on the phase precision and the QFI. Regarding phase sensitivity, multi-PSS on mode a demonstrates superior performance overall under certain parameters, at-

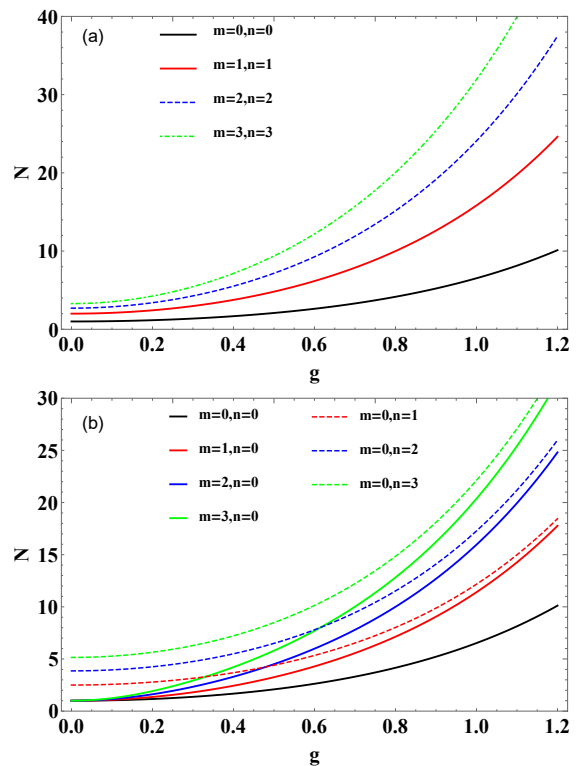


FIG. 11. The total mean photon number N as a function of g , with $\alpha = 1$. (a) symmetrical two-mode multi-PSS, (b) single mode multi-PSS.

tributed to homodyne detection on the mode a of the output. Furthermore, in the presence of internal photon losses, the multi-PSS exhibits better performance on mode b when the losses are substantial, while the opposite is true in the other case. In terms of the QFI, the multi-PSS performs better on mode b than on mode a .

In summary, the multi-PSS plays a role in overcoming the internal photon losses in SU(1,1) interferometers and in improving the accuracy of quantum measurements. This study underscores the potential of the multi-PSS as a valuable tool for improving the performance of quantum metrology and information processing systems.

ACKNOWLEDGMENTS

This work is supported by the National Natural Science Foundation of China (Grants No. 11964013 and No. 12104195) and the Training Program for Academic and Technical Leaders of Major Disciplines in Jiangxi Province (No. 20204BCJL22053).

APPENDIX A : THE PHASE SENSITIVITY OF MULTI-PSS

In this Appendix, we give the calculation formulas of

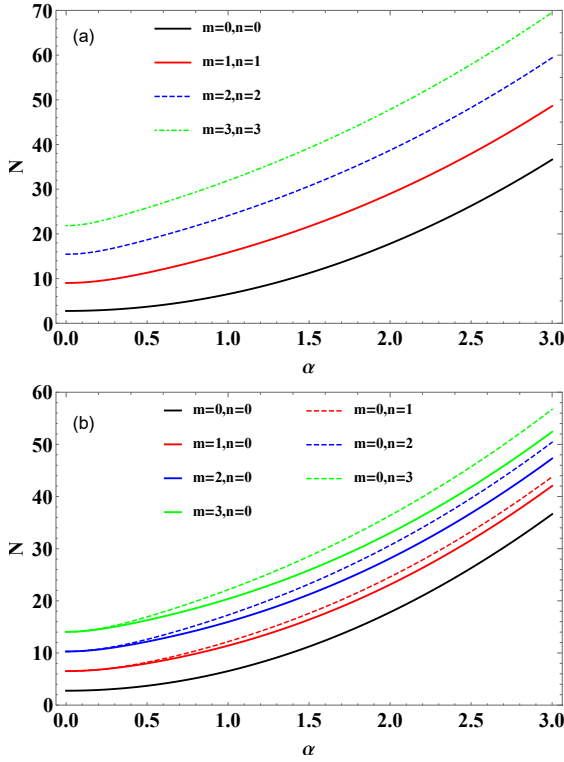


FIG. 12. The total mean photon number N as a function of α , with $g = 1$. (a) symmetrical two-mode multi-PSS, (b) single mode multi-PSS.

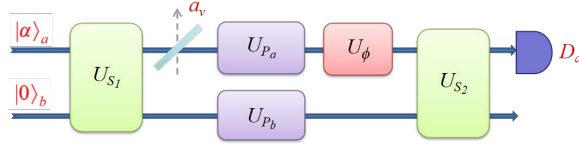


FIG. 13. Schematic diagram of the photon losses on mode a . the losses occurs before the multi-PSS.

the phase sensitivity for multi-PSS as follows

$$\Delta\phi = \frac{\sqrt{\langle \Psi_{out}^1 | X^2 | \Psi_{out}^1 \rangle - \langle \Psi_{out}^1 | X | \Psi_{out}^1 \rangle^2}}{|\partial \langle \Psi_{out}^1 | X | \Psi_{out}^1 \rangle / \partial \phi|}. \quad (\text{A1})$$

The output state $|\Psi_{out}^1\rangle$ is given by equation (2) in our paper, so the expectations related to the phase sensitivity for multi-PSS are specifically calculated as [43]

$$\begin{aligned} & \langle \Psi_{out}^1 | X | \Psi_{out}^1 \rangle \\ &= A^2 [e^{-i\phi} \cosh g D_{m_1+1, n_1, m_2, n_2} e^{w_1} \\ &+ \sinh g D_{m_1, n_1, m_2, n_2+1} e^{w_1} \\ &+ e^{i\phi} \cosh g D_{m_1, n_1, m_2+1, n_2} e^{w_1} \\ &+ \sinh g D_{m_1, n_1+1, m_2, n_2} e^{w_1}], \end{aligned} \quad (\text{A2})$$

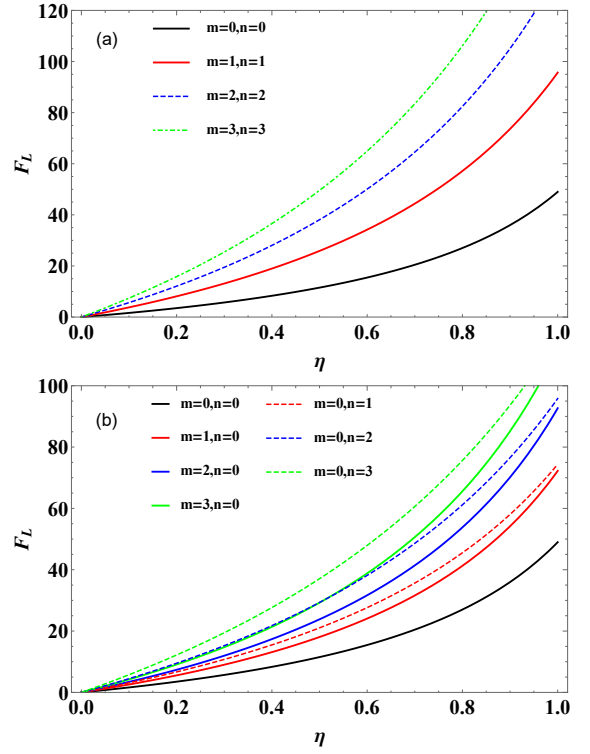


FIG. 14. The F_L as a function of transmittance η , with $g = 1$ and $\alpha = 1$. (a) symmetrical two-mode multi-PSS, (b) single mode multi-PSS.

and

$$\begin{aligned} & \langle \Psi_{out}^1 | X^2 | \Psi_{out}^1 \rangle \\ &= A^2 [e^{-2i\phi} \cosh^2 g D_{m_1+2, n_1, m_2, n_2} e^{w_1} \\ &+ e^{-i\phi} \sinh(2g) D_{m_1+1, n_1, m_2, n_2+1} e^{w_1} \\ &+ \sinh^2 g D_{m_1, n_1, m_2, n_2+2} e^{w_1} \\ &+ e^{2i\phi} \cosh^2 g D_{m_1, n_1, m_2+2, n_2} e^{w_1} \\ &+ e^{i\phi} \sinh(2g) D_{m_1, n_1+1, m_2+1, n_2} e^{w_1} \\ &+ \sinh^2 g D_{m_1, n_1+2, m_2, n_2} e^{w_1} \\ &+ 2 \cosh^2 g D_{m_1+1, n_1, m_2+1, n_2} e^{w_1} \\ &+ e^{-i\phi} \sinh(2g) D_{m_1+1, n_1+1, m_2, n_2} e^{w_1} \\ &+ e^{i\phi} \sinh(2g) D_{m_1, n_1, m_2+1, n_2+1} e^{w_1} \\ &+ 2 \sinh^2 g D_{m_1, n_1+1, m_2, n_2+1} e^{w_1}] \\ &+ \cosh(2g). \end{aligned}$$

APPENDIX B : THE QFI OF PHOTON LOSSES

The quantum state of the input state passing through the first OPA is denoted as $|\psi\rangle = U_{S1} |\alpha\rangle_a \otimes |0\rangle_b$, and its corresponding density operator is represented as ρ_0 , which satisfies the following relation

$$\text{Tr} \rho_0 = 1. \quad (\text{B1})$$

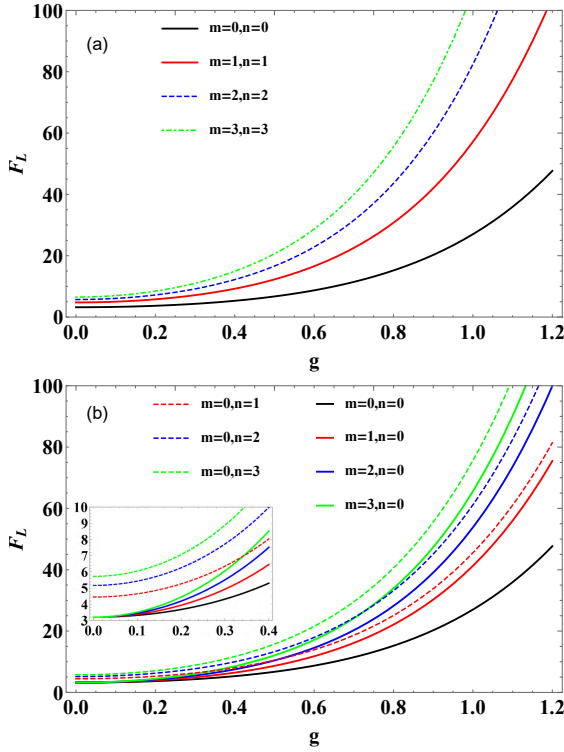


FIG. 15. The F_L as a function of g , with $\alpha = 1$ and $\eta = 0.8$. (a) symmetrical two-mode multi-PSS, (b) single mode multi-PSS.

The density matrix corresponding to the quantum state $U_{B_a} |\psi\rangle$ of $|\psi\rangle$ after experiencing photon losses is ρ

$$\rho = \sum_l \Pi_l(\eta) \rho_0 \Pi_l^\dagger(\eta), \quad (\text{B2})$$

where $\Pi_l(\eta)$ represents the Kraus operator, i.e.,

$$\Pi_l(\eta) = \sqrt{\frac{(1-\eta)^l}{l!}} \eta^{\frac{n}{2}} a^l. \quad (\text{B3})$$

It satisfies

$$\text{Tr} \rho = 1, \sum_l \Pi_l^\dagger(\eta) \Pi_l(\eta) = 1. \quad (\text{B4})$$

The quantum state of $U_{B_a} |\psi\rangle$ after photon subtraction operation can be expressed as $A' U_P U_{B_a} |\psi\rangle = A' a^m b^m U_{B_a} |\psi\rangle$, where A' is the normalization factor. Its density operator ρ' is

$$\begin{aligned} \rho' &= A'^2 a^m b^m \rho_0 b^{\dagger m} a^{\dagger m} \\ &= \sum_l \Pi_l(\eta) \rho'_0 \Pi_l^\dagger(\eta), \end{aligned} \quad (\text{B5})$$

which satisfies $\text{Tr} \rho' = 1$. Here $\rho'_0 = A'^2 \eta^m a^m b^m \rho_0 b^{\dagger m} a^{\dagger m} = A'^2 \eta^m U_P |\psi\rangle \langle \psi| U_P^\dagger = |\psi'\rangle \langle \psi'|$ is the density operator corresponding to the quantum state $|\psi'\rangle$ after the input state passes through the first

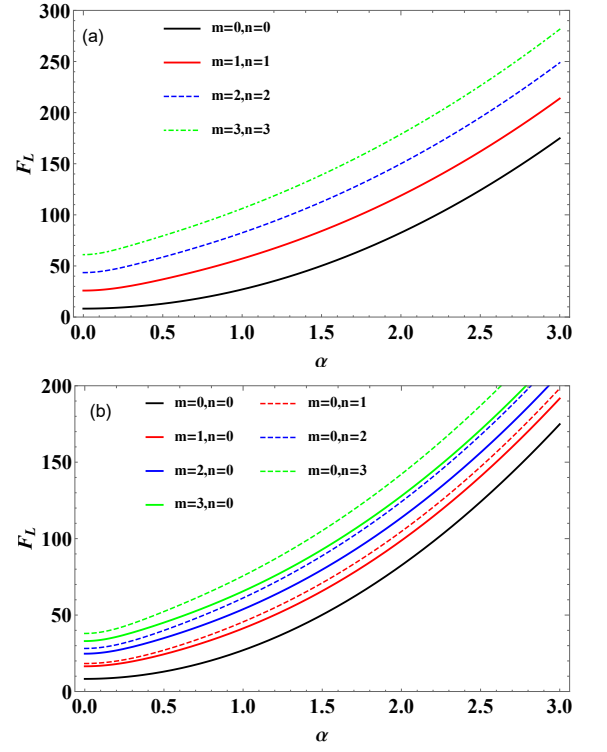


FIG. 16. The F_L as a function of α , with $g = 1$ and $\eta = 0.8$. (a) symmetrical two-mode multi-PSS, (b) single mode multi-PSS.

OPA and then through photon subtraction, and ρ'_0 also satisfies $\text{Tr} \rho'_0 = 1$. $A' \eta^{\frac{m}{2}}$ is the normalization factor of $|\psi'\rangle$

$$A'^2 \eta^m = A_0^2, \quad (\text{B6})$$

and A_0 reduces to A for $T_k = 1$. These derivations above utilize the following equations

$$\eta^{\frac{n}{2}} a^{\dagger m} = \eta^{\frac{m}{2}} a^{\dagger m} \eta^{\frac{n}{2}}, \quad (\text{B7})$$

$$a^m \eta^{\frac{n}{2}} = \eta^{\frac{m}{2}} \eta^{\frac{n}{2}} a^m. \quad (\text{B8})$$

The density operator ρ' is equivalent to the density operator of the quantum state obtained by first passing the input state through the first OPA, then performing photon subtraction, and finally experiencing photon losses (i.e. $|\psi'\rangle$, the quantum state after photon losses). We consider the phase shifter operator $e^{i\phi(a^\dagger a)} = e^{i\phi n}$ and introduce the parameter λ , which accounts for the selection of whether photon losses occurs before or after the phase shifter. Specifically, for $\lambda = 0$, it corresponds to photon losses occurring before the phase shifter, and for $\lambda = -1$, it corresponds to photon losses occurring after the phase shifter.

Next, we define the Kraus operator

$$\Pi_l(\phi, \eta, \lambda) = \sqrt{\frac{(1-\eta)^l}{l!}} e^{i\phi(n-\lambda l)} \eta^{\frac{n}{2}} a^l, \quad (\text{B9})$$

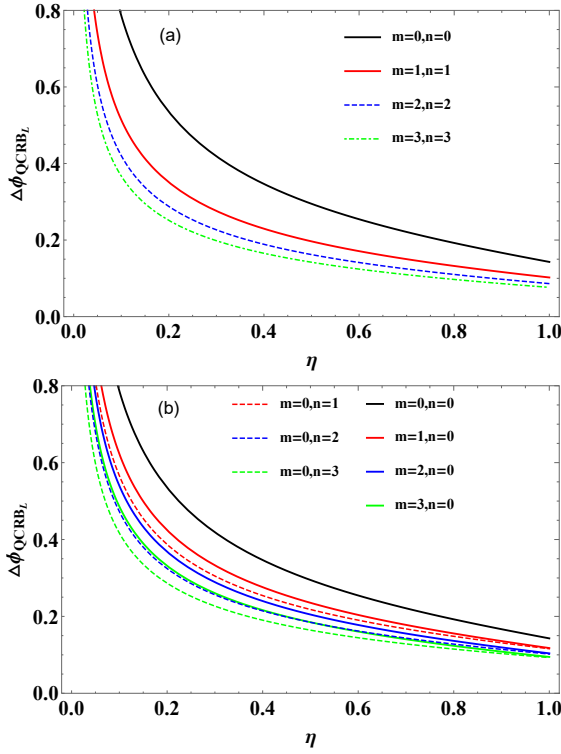


FIG. 17. The $\Delta\phi_{QCRB_L}$ as a function of transmittance η , with $g = 1$ and $\alpha = 1$. (a) symmetrical two-mode multi-PSS, (b) single mode multi-PSS.

and it satisfies

$$\sum_l \Pi_l^\dagger(\phi, \eta, \lambda) \Pi_l(\phi, \eta, \lambda) = 1. \quad (\text{B10})$$

Hence, in the case of photon losses, the density operator

corresponding to the quantum state of $|\psi'\rangle$ after passing through a phase shifter satisfies

$$\rho' \rightarrow \sum_l \Pi_l(\phi, \eta, \lambda) \rho'_0 \Pi_l^\dagger(\phi, \eta, \lambda). \quad (\text{B11})$$

The consistency between the form of this density operator and the Kraus operators $\Pi_l(\phi, \eta, \lambda)$, $\rho(x)$ and $\Pi_l(x)$ in Ref. [56], allows for the utilization of the corresponding formulas.

$$F_L \leq C_Q = 4 \left[\langle H_1 \rangle - \langle H_2 \rangle^2 \right], \quad (\text{B12})$$

where

$$H_1 = \sum_l \frac{d\Pi_l^\dagger(\phi, \eta, \lambda)}{d\phi} \frac{d\Pi_l(\phi, \eta, \lambda)}{d\phi}, \quad (\text{B13})$$

$$H_2 = i \sum_l \frac{d\Pi_l^\dagger(\phi, \eta, \lambda)}{d\phi} \Pi_l(\phi, \eta, \lambda), \quad (\text{B14})$$

and

$$\begin{aligned} F_L &= \frac{4\eta \langle n_0 \rangle \langle \Delta n^2 \rangle_0}{\langle \Delta n^2 \rangle_0 (1 - \eta) + \eta \langle n_0 \rangle} \\ &= \frac{4F\eta \langle n_0 \rangle}{(1 - \eta) F + 4\eta \langle n_0 \rangle}. \end{aligned} \quad (\text{B15})$$

For the multi-PSS with photon losses, the QFI can be obtained as

$$\begin{aligned} F_L &= \frac{4F\eta \langle \psi' | a^\dagger a | \psi' \rangle}{(1 - \eta) F + 4\eta \langle \psi' | a^\dagger a | \psi' \rangle} \\ &= \frac{4F\eta A_0^2 D_{m_1+1, n_1, m_2+1, n_2} e^{w_1}}{(1 - \eta) F + 4\eta A_0^2 D_{m_1+1, n_1, m_2+1, n_2} e^{w_1}}. \end{aligned} \quad (\text{B16})$$

-
- [1] A. N. Boto, P. Kok, D. S. Abrams, S. L. Braunstein, C. P. Williams, and J. P. Dowling, Quantum interferometric optical lithography: exploiting entanglement to beat the diffraction limit, *Phys. Rev. Lett.* 85(13), 2733 (2000).
- [2] J. J. Cooper, D. W. Hallwood, and J. A. Dunningham, Entanglement-enhanced atomic gyroscope, *Phys. Rev. A* 81(4), 043624 (2010).
- [3] W. Wasilewski, K. Jensen, H. Krauter, J. J. Renema, M. V. Balabas, and E. S. Polzik, Quantum noise limited and entanglement-assisted magnetometry, *Phys. Rev. Lett.* 104(13), 133601 (2010).
- [4] F. Dolde et al., Electric-field sensing using single diamond spins, *Nat. Phys.* 7(6), 459 (2011).
- [5] H. Muntinga et al., Interferometry with Bose-Einstein condensates in microgravity, *Phys. Rev. Lett.* 110(9), 093602 (2013).
- [6] C. F. Ockeloen, R. Schmied, M. F. Riedel, and P. Treutlein, Quantum metrology with a scanning probe atom interferometer, *Phys. Rev. Lett.* 111(14), 143001 (2013).
- [7] K. Liu, C. Cai, J. Li, L. Ma, H. Sun, and J. Gao, Squeezing-enhanced rotating-angle measurement beyond the quantum limit, *Appl. Phys. Lett.* 113(26), 261103 (2018).
- [8] Y. Zhai, Z. Yue, L. Li, and Y. Liu, Progress and applications of quantum precision measurement based on SERF effect, *Front. Phys.* 10, 969129 (2022).
- [9] Y. Wu, J. Guo, X. Feng, L. Q. Chen, C. H. Yuan, and W. Zhang, Atom-light Hybrid quantum gyroscope, *Phys. Rev. Applied* 14(6), 064023 (2020).
- [10] B. Yurke, S. L. McCall, and J. R. Klauder, SU(2) and SU(1,1) interferometers, *Phys. Rev. A* 33(6), 4033 (1986).
- [11] J. Kong, F. Hudelist, Z. Y. Ou, and W. Zhang, Cancellation of internal quantum noise of an amplifier by quantum correlation, *Phys. Rev. Lett.* 111(3), 033608 (2013).
- [12] C. M. Caves, Reframing SU(1,1) interferometry, *Adv. Quantum Technol.* 3(11), 1900138 (2020).
- [13] J. Jing, C. Liu, Z. Zhou, Z. Y. Ou, and W. Zhang, Realization of a nonlinear interferometer with parametric amplifiers, *Appl. Phys. Lett.* 99(1), 011110 (2011).
- [14] J. Kong, Z. Y. Ou, and W. Zhang, Phase-measurement sen-

- sitivity beyond the standard quantum limit in an interferometer consisting of a parametric amplifier and a beam splitter, *Phys. Rev. A* 87(2), 023825 (2013).
- [15] B. Chen, C. Qiu, S. Chen, J. Guo, L. Q. Chen, Z. Y. Ou, and W. Zhang, Atom-light hybrid interferometer, *Phys. Rev. Lett.* 115(4), 043602 (2015).
- [16] B. E. Anderson, P. Gupta, B. L. Schmittberger, T. Horrom, C. Hermann-Avigliano, K. M. Jones, and P. D. Lett, Phase sensing beyond the standard quantum limit with a variation on the SU(1, 1) interferometer, *Optica* 4(7), 752–756 (2017).
- [17] S. S. Szigeti, R. J. Lewis-Swan, and S. A. Haine, Pumped-up SU(1, 1) interferometry, *Phys. Rev. Lett.* 118(15), 150401 (2017).
- [18] G. Frascella, E. E. Mikhailov, N. Takanashi, R. V. Zakharov, O. V. Tikhonova, and M. V. Chekhova, Wide-field SU(1,1) interferometer, *Optica* 6(9), 1233–1236 (2019).
- [19] J. Liu, Y. Wang, M. Zhang, J. Wang, D. Wei, and H. Gao, Ultra-sensitive phase measurement based on an SU(1, 1) interferometer employing external resources and subtract intensity detection, *Opt. Express* 28(26), 39443–39452 (2020).
- [20] W. Du, J. F. Chen, Z. Y. Ou, and W. Zhang, Quantum dense metrology by an SU(2)-in-SU(1, 1) nested interferometer, *Appl. Phys. Lett.* 117(2), 024003 (2020).
- [21] D. Liao, J. Xin, and J. Jing, Nonlinear interferometer based on two-port feedback nondegenerate optical parametric amplification, *Opt. Commun.* 496, 127137 (2021).
- [22] A. M. Marino, N. V. Corzo Trejo, and P. D. Lett, Effect of losses on the performance of an SU(1,1) interferometer, *Phys. Rev. A* 86(2), 023844 (2012).
- [23] D. Li, C. H. Yuan, Z. Y. Ou, and W. Zhang, The phase sensitivity of an su(1, 1) interferometer with coherent and squeezed-vacuum light, *New J. Phys.* 16(7), 073020 (2014).
- [24] M. Manceau, G. Leuchs, F. Khalili, and M. Chekhova, Detection loss tolerant supersensitive phase measurement with an SU(1,1) interferometer, *Phys. Rev. Lett.* 119(22), 223604 (2017).
- [25] M. S. Kim, Recent developments in photon-level operations on travelling light fields, *J. Phys. B: At., Mol. Opt. Phys.* 41(13), 133001 (2008).
- [26] V. Parigi, A. Zavatta, M. Kim, and M. Bellini, Probing quantum commutation rules by addition and subtraction of single photons to/from a light field, *Science* 317(5846), 1890–1893 (2007).
- [27] M. Bellini and A. Zavatta, Manipulating light states by single-photon addition and subtraction, *Prog. Opt.* 55, 41–83 (2010).
- [28] P. S. Yan, L. Zhou, W. Zhong, and Y. B. Sheng, Advances in quantum entanglement purification, *Sci. China-Phys. Mech. Astron.* 66(5), 250301 (2023).
- [29] C. H. Bennett, H. J. Bernstein, S. Popescu, and B. Schumacher, Concentrating partial entanglement by local operations, *Phys. Rev. A* 53(4), 2046 (1996).
- [30] R. Horodecki, P. Horodecki, M. Horodecki, and K. Horodecki, Quantum entanglement, *Rev. Mod. Phys.* 81(2), 865 (2009).
- [31] S. L. Braunstein and P. van Loock, Quantum information with continuous variables, *Rev. Mod. Phys.* 77(2), 513 (2005).
- [32] P. G. Kwiat, S. Barraza-Lopez, A. Stefanov, and N. Gisin, Experimental entanglement distillation and 'hidden' non-locality, *Nature* 409(6823), 1014–1017 (2001).
- [33] L. L. Guo, Y. F. Yu, and Z. M. Zhang, Improving the phase sensitivity of an SU(1,1) interferometer with photon-added squeezed vacuum light, *Opt. Express* 26(22), 29099 (2018).
- [34] K. Zhang, Y. H. Lv, Y. Guo, J. T. Jing, and W. M. Liu, Enhancing the precision of a phase measurement through phase-sensitive non-Gaussianity, *Phys. Rev. A* 105(4), 042607 (2022).
- [35] Y. K. Xu, S. K. Chang, C. J. Liu, L. Y. Hu, and S. Q. Liu, Phase estimation of an SU(1,1) interferometer with a coherent superposition squeezed vacuum in a realistic case, *Opt. Express* 30(21), 38178 (2022).
- [36] A. Zavatta, V. Parigi, M. S. Kim, H. Jeong, and M. Bellini, Experimental demonstration of the Bosonic commutation relation via superpositions of quantum operations on thermal light fields, *Phys. Rev. Lett.* 103(14), 140406 (2009).
- [37] M. V. Chekhova and Z. Y. Ou, Nonlinear interferometers in quantum optics, *Adv. Opt. Photonics* 8(1), 252890 (2016).
- [38] H. Ma and Y. Liu, Super-resolution localization microscopy: Toward high throughput, high quality, and low cost, *APL Photonics* 5(6), 080902 (2020).
- [39] Z. Y. Ou, Enhancement of the phase-measurement sensitivity beyond the standard quantum limit by a nonlinear interferometer, *Phys. Rev. A* 85(2), 023815 (2012).
- [40] J. Xin, Phase sensitivity enhancement for the SU(1,1) interferometer using photon level operations, *Opt. Express* 29(26), 43970–43984 (2021).
- [41] C. W. Helstrom, Minimum mean-squared error of estimates in quantum statistics, *Phys. Lett. A* 25(2), 101 (1967).
- [42] C. W. Helstrom, Quantum detection and estimation theory, *J. Stat. Phys.* 1(2), 231 (1969).
- [43] Y. Xu, T. Zhao, Q. Kang, C. Liu, L. Hu, and S. Liu, Phase sensitivity of an SU(1,1) interferometer in photon-loss via photon operations, *Opt. Express* 31(5), 8414 (2023).
- [44] M. Xiao, L. A. Wu, and H. J. Kimble, Precision measurement beyond the shot-noise limit, *Phys. Rev. Lett.* 59(3), 278 (1987).
- [45] R. Demkowicz-Dobrzański, M. Jarzyna, and J. Kołodyński, Quantum limits in optical interferometry, *Prog. Optics* 60, 345–435 (2015).
- [46] M. Bradshaw, P. K. Lam, and S. M. Assad, Ultimate precision of joint quadrature parameter estimation with a Gaussian probe, *Phys. Rev. A* 97(1), 012106 (2018).
- [47] D. Li, C. H. Yuan, Z. Y. Ou, and W. Zhang, The phase sensitivity of an SU(1,1) interferometer with coherent and squeezed-vacuum light, *New J. Phys.* 16(7), 073020 (2014).
- [48] X. Y. Hu, C. P. Wei, Y. F. Yu, and Z. M. Zhang, Enhanced phase sensitivity of an SU(1,1) interferometer with displaced squeezed vacuum light, *Front. Phys.* 11(3), 114203 (2016).
- [49] P. M. Anisimov, G. M. Raterman, A. Chiruvelli, W. N. Plick, S. D. Huver, H. Lee, and J. P. Dowling, Quantum metrology with two-mode squeezed vacuum: parity detection beats the Heisenberg limit, *Phys. Rev. Lett.* 104(10), 103602 (2010).
- [50] D. Li, B. T. Gard, Y. Gao, C. H. Yuan, W. Zhang, H. Lee, and J. P. Dowling, Phase sensitivity at the Heisenberg limit in an SU(1,1) interferometer via parity detection, *Phys. Rev. A* 94(6), 063840 (2016).
- [51] S. Ataman, A. Preda, and R. Ionicioiu, Phase sensitivity of

- a Mach-Zehnder interferometer with single-intensity and difference-intensity detection, *Phys. Rev. A* 98(4), 043856 (2018).
- [52] D. Li, C. H. Yuan, Y. Yao, W. Jiang, M. Li, and W. Zhang, Effects of loss on the phase sensitivity with parity detection in an $SU(1,1)$ interferometer, *J. Opt. Soc. Am. B* 35(5), 309106 (2018).
- [53] C. M. Caves, Quantum-mechanical noise in an interferometer, *Phys. Rev. D* 23(8), 1693 (1981).
- [54] O. Assaf and Y. Ben-Aryeh, Quantum mechanical noise in coherent-state and squeezed-state Michelson interferometers, *J. Opt. B: Quantum Semiclass. Opt.* 4(1), 49 (2002).
- [55] J. Beltran and A. Luis, Breaking the Heisenberg limit with inefficient detectors, *Phys. Rev. A* 72(4), 045801 (2005).
- [56] B. M. Escher, R. L. de Matos Filho, and L. Davidovich, General framework for estimating the ultimate precision limit in noisy quantum-enhanced metrology, *Nat. Phys.* 7(5), 406 (2011).
- [57] Helstrom C W, *Quantum detection and estimation theory* (Academic, 1976), 123.
- [58] S. K. Chang, W. Ye, H. Zhang, L. Y. Hu, J. H. Huang, and S. Q. Liu, Improvement of phase sensitivity in an $SU(1, 1)$ interferometer via a phase shift induced by a Kerr medium, *Phys. Rev. A* 105(3), 033704 (2022).
- [59] S. K. Chang, C. P. Wei, H. Zhang, Y. Xia, W. Ye, and L. Y. Hu, Enhanced phase sensitivity with a nonconventional interferometer and nonlinear phase shifter, *Phys. Lett. A* 384(29), 126755 (2020).